

## Tropical Intraseasonal Oscillation, Super Cloud Clusters, and Cumulus Convection Schemes. Part II: 3D Aquaplanet Simulations

WINSTON C. CHAO

*Laboratory for Atmospheres, NASA/Goddard Space Flight Center, Greenbelt, Maryland*

LITAO DENG

*Space Applications Corporation, Vienna, Virginia*

(Manuscript received 19 April 1996, in final form 19 March 1997)

### ABSTRACT

Chao and Lin's work on tropical intraseasonal oscillations, super cloud clusters, and cumulus convection schemes is extended from a 2D model setup to a 3D aquaplanet setup. It is found that super cloud clusters can be simulated in a 3D model and that the 3D setup has more stringent requirements on the cumulus convection scheme than the 2D setup does for a successful simulation of super cloud clusters. Three cumulus convection schemes are compared in experiments simulating super cloud clusters. In the more successful experiments, individual cloud cluster pairs in the meridional direction, once generated near the equator by the cloud cluster tele-induction mechanism, assume a poleward movement while exhibiting weak zonal movement. The combination of two or three successive cloud cluster pairs (i.e., vortex pairs) straddling the equator gives rise to westerly wind burst events of sizable longitudinal range and duration. Thus, the westerly wind burst, as appeared in the model, is really a part of the super cloud cluster structure. The evaporation–surface wind feedback mechanism is found to be unnecessary for the existence of the super cloud clusters. However, it does make the latter more robust. The need for improvement in cumulus parameterization for tropical simulation is discussed.

### 1. Introduction

The tropical intraseasonal oscillation of 40–50 day period, also known as the Madden–Julian (1971, 1972) oscillation (MJO), has been the topic of many investigations for reasons of both physical interest and practical forecast application (Ferranti et al. 1990). For a review of the observational studies of MJO, the reader is referred to Madden and Julian (1994). Among the more recent observational works are Salby and Hendon (1994), Hendon and Salby (1994), and Hendon and Liebmann (1994). For a concise review of theoretical work on the MJO, the reader is referred to Hayashi and Golder (1993) and Kuma (1994). Among the recent theoretical work are Emanuel et al. (1994), Neelin and Yu (1994), and Yu and Neelin (1994). The interpretation of the origin of the MJO has greatly interested the research community. Until recently, the most popular foundation for interpreting the MJO has been the wave–CISK mechanism and its variants (Chao 1987; Lau and Peng 1987; Hendon 1988; Chang and Lim 1988; among others). However, the difficulties encountered in simu-

lations based on the wave–CISK mechanism, that is, the excessive speed and the preference for the smallest scale of the associated convective region, have been obvious. Chao (1995), while acknowledging the importance of the interaction between convection and convection-induced large-scale circulation, discussed these difficulties and attributed their cause to the particular cumulus convection formulation used in wave–CISK type of simulations, which depends on the vertical velocity at the top of the boundary layer and has a fixed vertical heating profile. Another mechanism proposed for the MJO is that of the evaporation–surface wind feedback, which was later renamed the wind-induced surface heat exchange (WISHE) mechanism (Emanuel 1987; Neelin et al. 1987). This mechanism will be discussed in the context of our numerical experiments.

In Part I of this paper (Chao and Lin 1994, hereafter CL), a new framework for interpreting the MJO was proposed. Chao and Lin interpret the MJO as the tropical circulation driven by a convective region over the equatorial region of the size of 30–40 degrees in longitude. In the most common cases this convective region arises in the western Indian Ocean and moves eastward a distance of one-third of the globe to the mid-Pacific, where SST is relatively high, in about 40–50 days and is followed by a new convective region arising in the western Indian Ocean to repeat the cycle. This convective region

---

*Corresponding author address:* Dr. Winston C. Chao, Mail Code 913, NASA/GSFC, Greenbelt, MD 20771.  
E-mail: winston.chao@gsfc.nasa.gov

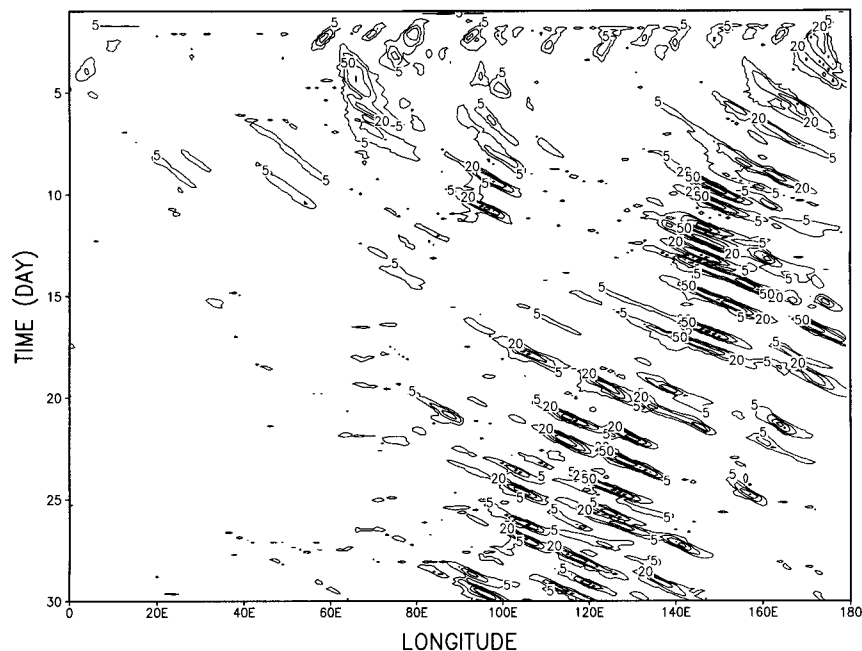


FIG. 1. The precipitation field of an experiment identical to Fig. 8 of CL except that the direction of the basic flow, toward which the zonally averaged  $u$  wind is relaxed in the Rayleigh friction term, is reversed.

is composed of one or more super cloud clusters (Nakazawa 1988; Lau et al. 1991; Sui and Lau 1992). A super cloud cluster is the envelope, or wave packet, of successive *well-separated* cloud clusters (Fig. 5 of Nakazawa 1988; CL have argued that super cloud clusters should be identified as solitary waves.) The speed and often the direction of the envelope are different from those of the individual cloud clusters. Thus, to understand the origin of MJO, one has to understand the origin of the super cloud clusters and their eastward movement and speed. According to CL, the latter two items can be understood as follows. A super cloud cluster comprises successive individual cloud clusters arising at or close to the equator on the upstream side (east side, in a basic easterly) of existing cloud clusters. The sudden rise of a cloud cluster sets off gravity waves propagating in all directions. Since the moisture field is not uniform surrounding the cloud cluster with the upstream side near or at the equator having more low-level moisture (simply because the moisture on the upstream side has not been “used” by the cloud cluster; this will also be discussed along with Fig. 13d), the gravity waves can set off a new cloud cluster more easily there. Chao and Lin called this process *the cloud cluster teleinduction mechanism*, which is simulated in CL’s 2D (longitude–height) model. Occasionally in CL’s 2D model, as an alternative and less frequent way of setting off a new cloud cluster, the convective cooling due to evaporation of falling rain on a cloud cluster drives a mesoscale downward motion that forces the boundary layer air to move in all directions. The upstream branch creates a

convergence on the upstream side of the existing cloud cluster. The boundary layer convergence, combined with the high moisture content on the upstream side, initiates a new cloud cluster. In CL’s 2D simulation once a new cloud cluster is generated, it competes for moisture supply with the existing one and leads to the demise of the latter. The individual cloud cluster moves downstream relative to the basic flow speed to maximize its life span (about 2–3 days). The successive formation of new cloud clusters on the upstream side (i.e., a chain reaction) and the downstream movement and the demise of the existing ones give rise to an envelope, which is the super cloud cluster.

Based on this theory we can make two predictions: One is that, if the basic flow reverses direction, the super cloud cluster should also reverse its direction and, if the basic flow is set at zero, no super cloud cluster can appear. The other is that, if we can somehow make the rise of the cloud cluster more sluggish, the super cloud cluster will not appear in the model. The first one is quite obvious and was verified in a simple experiment by changing the direction of the prescribed winds toward which the Rayleigh friction adjusts the zonally averaged flow and in a separate experiment by setting the prescribed winds to zero. The results for these experiments are shown in Figs. 1 and 2. To verify the second prediction, we added a sizable divergence damping in the momentum equation to suppress interaction between convective heating and circulation (thereby suppressing the fast growth of cloud cluster) and repeated the 2D experiment with the Manabe et al. (1965)

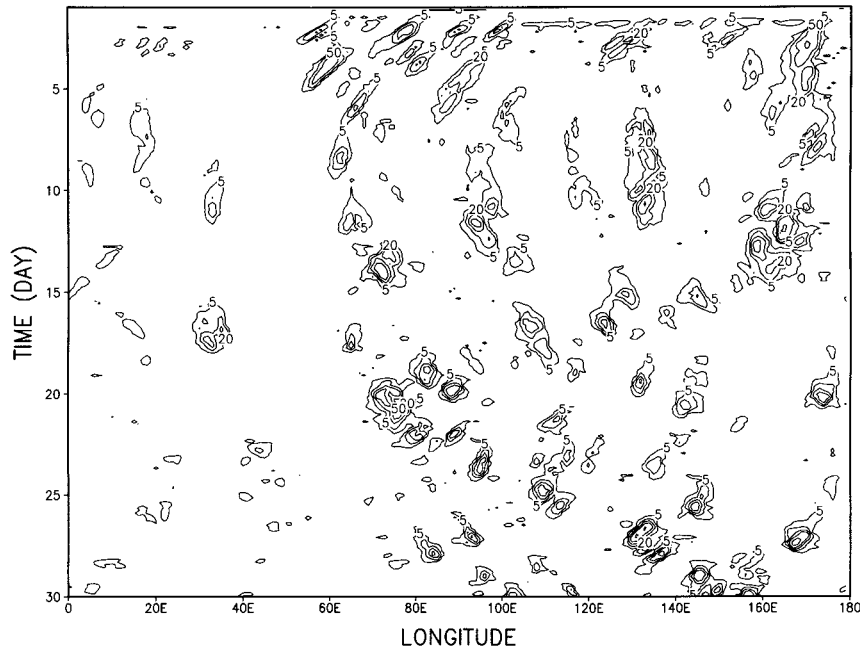


FIG. 2. The precipitation field of an experiment identical to Fig. 8 of CL except that the zonally averaged  $u$  wind is restored to zero.

convective adjustment scheme. That is,  $\partial \mathbf{V} / \partial t = \dots + f_{\text{div}} \nabla D$ , where  $f_{\text{div}} = f_d l^2 \Delta t^{-1}$ ,  $f_d = 0.4$ ,  $l$  is the zonal grid size,  $\Delta t$  is the time step, and  $D$  is the divergence (cf. Talagrand 1972). The results (Fig. 3) show that the super cloud cluster structure can no longer be maintained.

Chao and Lin's 2D model simulations obtained results very closely resembling observed super cloud clusters (Nakazawa 1988). They also pointed out that the simulation results are highly sensitive to the cumulus convective scheme used. Of the four convection schemes used, only two were able to simulate the super cloud

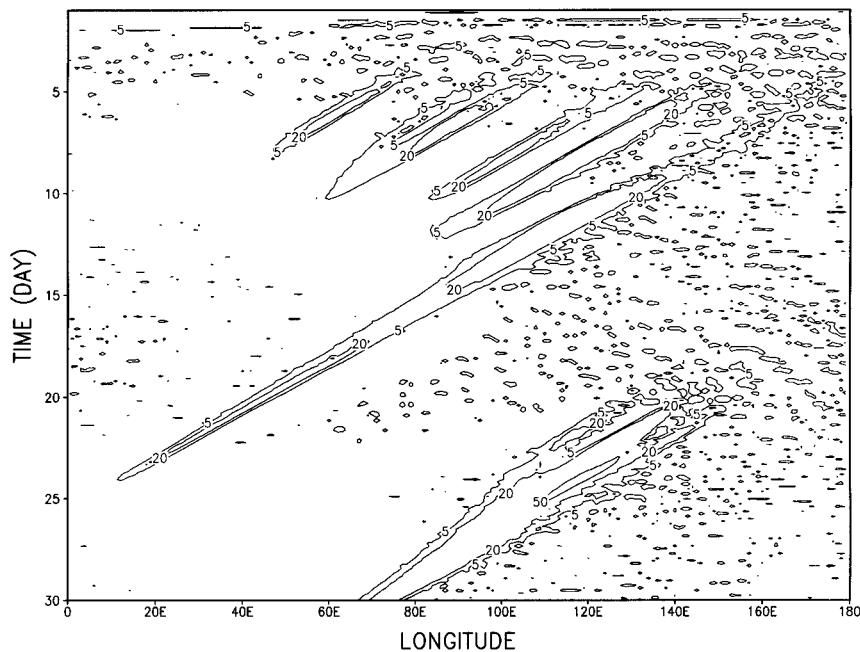


FIG. 3. The precipitation field of an experiment identical to Fig. 8 of CL except that a sizable divergence damping in the momentum equation is introduced.

clusters. Chao and Lin's work provides a framework for a more comprehensive interpretation of the MJO. The work ahead is still formidable. For example, the splitting of a new convective region from the convective region associated with the MJO in the Indian Ocean and its subsequent northward movement (Yasunari 1981) have no satisfactory explanation. Also, the movement of the convective region from the Indian Ocean to the mid-Pacific is not continuous (Zhu and Wang 1993; Lau et al. 1996). Moreover, not too infrequently the convective region associated with the tropical intraseasonal oscillation travels *westward* across the entire western Pacific and the Indian Ocean (Fig. 8 of Wang and Rui 1990). Before addressing these difficult problems it is best to take some intermediate steps in our attempt to gain a more complete understanding of the MJO.

As mentioned in CL, a logical first step to extend their work is to switch from the 2D model to a 3D model. The 3D convective circulation can be quite different from the 2D convective circulation. For instance, given the same intensity of the growth of a cloud cluster at a location, the 2D setup implies that a line of convection in the direction of the third dimension and thus at any fixed distance from this location it induces more vigorous gravity wave response than in the 3D setup (the gravity waves excited in a 3D model propagate in all horizontal directions and therefore their amplitudes diminish more rapidly). Thus a cumulus parameterization scheme that can simulate the cloud cluster tele-induction mechanism (and thus be successful in simulating the super cloud cluster) in a 2D setup may fail in a 3D setup. Thus the two successful convective schemes in the 2D setup, Manabe's convective adjustment scheme and the simple convective scheme described in CL, should be reexamined in the 3D setup. Besides, even if a scheme remains successful in simulating super cloud clusters in the 3D setup, the speed and other characteristics can be very different from those obtained in a 2D setup. The 3D setup allows the cloud clusters one extra dimension to move around and thus allows very different circulation field.

Three-dimensional GCM simulation of the MJO has been attempted by numerous investigators with varying degrees of success (Hayashi and Golder 1993; Park et al. 1990; Pitcher and Geisler 1987; Swinbank et al. 1988; Tokioka et al. 1988; Lau and Lau 1986; Slingo and Madden 1991). The successful simulation of the MJO should at least exhibit a period of 40–50 days in various fields. Included in this should be the movement of a precipitation region, comprising one or more super cloud clusters, from the Indian Ocean to the mid-Pacific in the same period as observed by Lau and Chen (1986). This is an important aspect that has not been demonstrated in any GCM. The full-feature GCM simulation has its own merits. However, for the purpose of interpretation of physical phenomena and for the purpose of understanding how simulations can be improved, a less complicated model can play a complementary role. This

is the direction we are taking. Specifically, we will use a simplified version of the Goddard Laboratory for Atmospheres General Circulation Model to investigate the convective activities on an aquaplanet with zonally uniform SST.

Similar aquaplanet simulations have been conducted by other research groups. Hayashi and Sumi (1986), using a T20 model with the Kuo parameterization scheme, obtained eastward-propagating (at a speed of  $15 \text{ m s}^{-1}$ ) convective regions. Their results showed wavenumber 1 features along with the individual convective region of 3000-km size. However, the internal structure of the super cloud cluster, that is, the westward propagating individual cloud clusters, was not simulated. Using a T42 model, Numaguti and Hayashi (1991a, b) extended Hayashi and Sumi's work and compared simulations with the Kuo scheme and those with the Manabe scheme (i.e., the moist convective adjustment scheme) and found that simulations with the Manabe scheme showed, in addition to the eastward (at  $8.5 \text{ m s}^{-1}$ ) movement of convective regions (the super cloud clusters), planetary-scale features. An important aspect of their results with the Manabe scheme, though not emphasized by them, is that the internal structure of super cloud clusters, that is, the westward propagating cloud clusters, appeared. Their results clearly demonstrated the dramatic impact the choice of convection scheme has on the modeled circulation pattern. Both Hayashi and Sumi (1986) and Numaguti and Hayashi (1991a, b) attributed the eastward movement of the modeled convective regions to the wave–CISK dynamics of Kelvin waves. The origin of the sensitivity to the convection scheme was not discussed in either paper. Recently, Kuma (1994) did a similar type of aquaplanet simulations with the Kuo scheme and also attributed the eastward movement to Kelvin wave–CISK. Also Yano et al. (1995), using a shallow-water model, have argued for WISHE as the mechanism for the eastward movement. These recent works will be commented on in the discussion section. In summary, the previous work on aquaplanet simulation has not resolved the question of why the convective region (at the synoptic and planetary scales) moves eastward. Also, it did not offer any interpretation for the high sensitivity to the choice of convection scheme.

Our work expands on the previous work. Although our numerical experiments have many similarities to the previous work, we offer a different interpretation as to the origin of the eastward movement of the convective regions. In addition, our results reveal the nature of westerly wind bursts as a feature of the internal structure of the super cloud cluster. We will first compare the behavior of the convective activity and the associated circulation field in the 3D model with those in the 2D model. The role of  $\beta$ , a basic feature of the 3D model, will be studied. We will also study the sensitivity of the model results to the choice of cumulus convection scheme and to the evaporation–surface wind feedback.

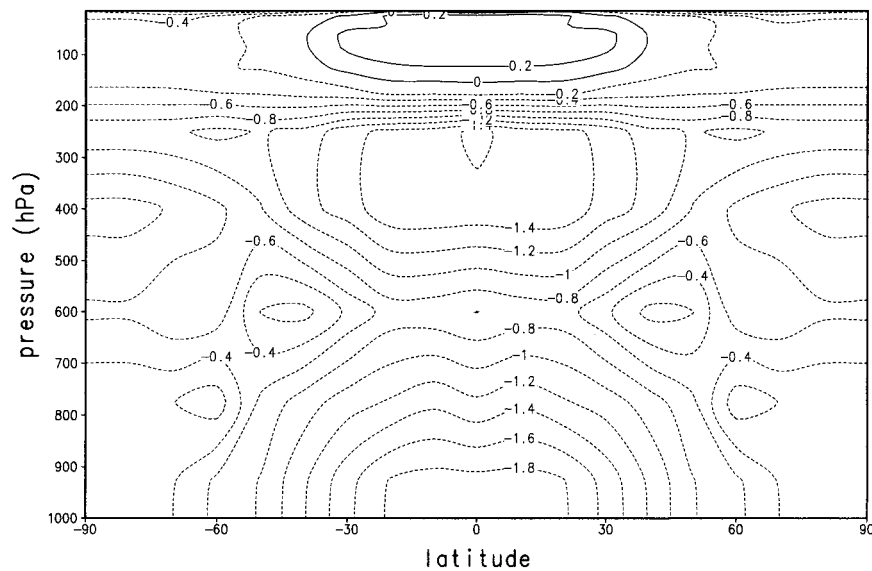


FIG. 4. The radiative cooling rate (in  $^{\circ}\text{C}/\text{day}$ ) used in the model.

We will offer some (speculative) discussions on the sensitivities to the choice of cumulus convection scheme. Our results will be compared with the previous work (Hayashi and Sumi 1986; Numaguti and Hayashi 1991a,b; Kuma 1994; Yano et al. 1995), but not in any great depth. To directly compare results from different models and to interpret the causes for the differences is very difficult due to the large differences among the models. Thus, we will mainly focus on the comparison of convection schemes under a single model.

## 2. Model description

The model used is a simplified version of the Goddard Laboratory for Atmospheres General Circulation Model (GLA GCM). It is the same model that CL used to set up their 2D model. The dynamics part of the model is a substantially revised version of the GLAS fourth-order model (Kalnay et al. 1983). The model uses a center fourth-order differencing scheme on the nonstaggered A grid in the horizontal and a second-order differencing scheme in the vertical. The flux-form spatial finite-differencing scheme formally conserves kinetic energy but not potential enstrophy. However, potential enstrophy is nearly conserved in practice. The vertical finite-differencing scheme is that of Arakawa and Suarez (1983). According to the design of this scheme, potential temperature (instead of temperature) is used as a prognostic variable. The locally consistent hydrostatic equation at the bottom level is a salient feature of this scheme. The time scheme is an initial Matsuno step followed by leap-frog steps. A polar filter (Takacs and Balgovid 1983) is applied to the time tendency of momentum and potential temperature. A fourth-order Shapiro filter is applied to momentum and potential temperature.

The moisture transport utilizes a second-order van

Leer-type scheme (Lin et al. 1994), which is conservative and monotonic. The monotonic constraint on the implied subgrid moisture distribution guarantees the positivity of the water-vapor mixing ratio without the need for an explicit diffusion (such as the Shapiro filter in the original design) and/or filling algorithm. Transport of moisture is done sequentially in each spatial direction. Since there is no need for spatial and time filters, this new scheme is just as fast as the original fourth-order finite-difference scheme.

The planetary boundary layer and vertical diffusion parameterizations follow those of the ECMWF GCM (Louis 1979). It uses the Monin–Obukhov similarity theory for surface flux calculation. Vertical diffusion coefficient is Richardson number dependent. For our limited modeling purpose the observed zonally averaged net radiative heating (Newell et al. 1972), Fig. 4, is used in lieu of the costly radiation parameterization. This simplification limits the realism of the experiments. In the quasi-equilibrium state of the model the sum of surface sensible heat flux and latent heat flux (evaporation) is determined by the total radiative cooling imposed. In the real atmosphere this is not true. However, since our objective is to investigate the interaction between convection and circulation, this simplification does not create a problem. Obviously, our model setup excludes any cloud–radiation feedback. This has the distinct advantage that whatever occurs in our model has nothing to do with cloud–radiation interaction.

The model has 12 sigma levels in the vertical. Table 1 gives the sigma values. The horizontal grids are latitude–longitude grids with  $1^{\circ}$  grid interval in the longitudinal direction. The grid interval in the latitudinal direction is variable with a uniform  $4^{\circ}$  poleward of  $30^{\circ}$  and a uniform  $1^{\circ}$  equatorward of  $10^{\circ}$  and smoothly varying in the transition region in between. In the transition

TABLE 1. Sigma values at the interface levels used in the model.

Level	Sigma
1	0.0
2	0.1
3	0.2
4	0.3
5	0.4
6	0.5
7	0.6
8	0.7
9	0.8
10	0.9
11	0.95
12	0.98
13	1.0

region the order of accuracy of the horizontal finite-differencing scheme is the first instead of the fourth. Such a varying interval grid has been used by Staniforth and Mitchell (1978) without any apparent ill effects. The time step for the dynamics part of the model is 2.5 min.

The SST (Fig. 5) is zonally uniform and symmetric with respect to the equator. The scope of this paper is limited to zonally uniform SST. The model, like most models, does not have realistic sensitivity to the SST zonal variation in the sense that when the observed SST is used the precipitation regions do not have realistic zonal extent (i.e., too narrow). This problem will be dealt with as a part of future research. The initial conditions are arbitrarily taken from the zonal and cross-equator average of the ECMWF analysis for 17 July 1981. The model is run with three different cumulus parameterization schemes: the Manabe et al. (1965) moist convective adjustment (MCA) scheme, the relaxed Arakawa-Schubert (RAS) scheme (Moorthi and Suarez 1992), which is a part of the GLA GCM, and the simple convective scheme of CL. The calling interval is 10 min for RAS and is 1 h for both the MCA scheme and the simple convective scheme. The heating and moistening rates from the convection scheme are saved and used at each dynamics time step until the next convection call.

In summary, our model remains the same as the GLA model with the modifications of an aquaplanet setting, prescribed radiative cooling rate with the exclusion of cloud-radiation interaction, a new moisture advection scheme, higher resolution in the Tropics, and the use of additional convection schemes. The purpose of these modifications is to facilitate our experiments.

### 3. The experiments

The first experiment, denoted by EMCA, is done with the MCA scheme. The integration lasts for 80 days. The initial 15 days is, judging from the precipitation output, a period of adjustment and is thus disregarded in our analysis. The zonally averaged precipitation averaged

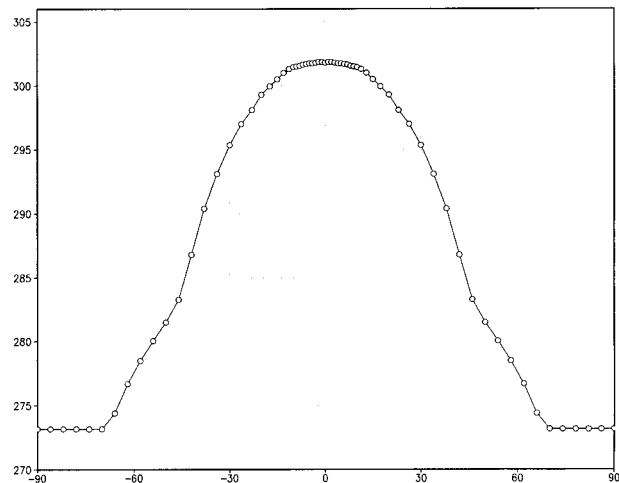


FIG. 5. The zonally uniform SST (K) as a function of latitude used in the model.

from day 22 to day 42, Fig. 6, shows an ITCZ right over the equator. The longitude-time distribution of precipitation averaged between 5°S and 5°N is given in Fig. 7. Between day 22 and day 42 there are two super cloud clusters. The one to the west fades after day 44. The one to the east becomes much more regular. Its speed ( $\sim 10 \text{ m s}^{-1}$ ) is such that it can cover a third of the globe in two weeks. Such speed is not unrealistic. Sui and Lau's (1992) Fig. 10 shows an observed super cloud cluster moving at about this speed. So does Nakazawa's (1988) Fig. 2. The frequency of the generation of new cloud clusters, about every 2 days, is quite realistic, judging from Nakazawa's (1988) observational findings. So is the 20° distance between the neighboring cloud clusters. In Fig. 7 each cloud cluster appears to last for less than 2 days and little westward movement

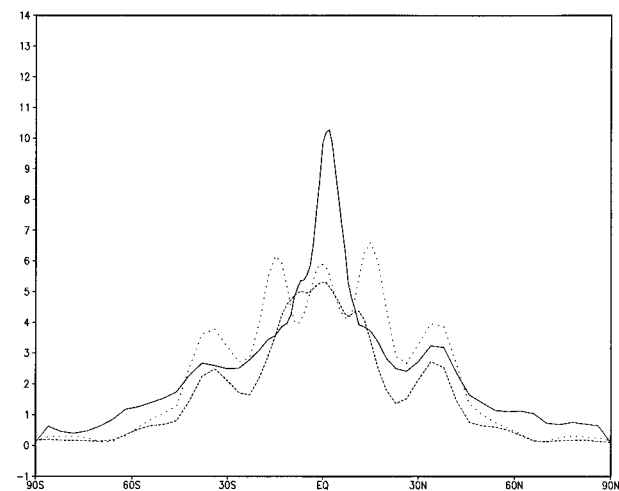


FIG. 6. The zonally averaged precipitation ( $\text{mm day}^{-1}$ ) averaged over day 20-40 in EMCA (solid), ERAS (dotted), and ECL (dashed).

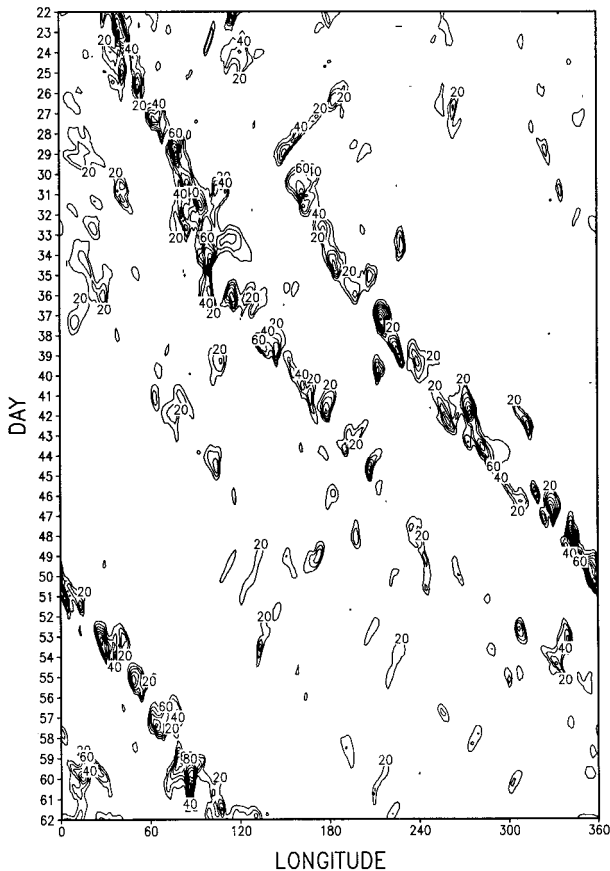


FIG. 7. The longitude–time distribution of precipitation ( $\text{mm day}^{-1}$ ) averaged between  $5^{\circ}\text{S}$  and  $5^{\circ}\text{N}$  in EMCA.

of the cloud clusters is exhibited. However, in a time sequence analysis of latitude–longitude distribution of precipitation we found that the cloud clusters, after forming over or near the equator, soon move poleward and at the same time assume little zonal movement (frequently a small eastward movement is found). The poleward and weak zonal movement explains the short duration of cloud clusters and lack of westward movement in Fig. 7, respectively. Figure 8 shows a typical time series event starting at hour 18 on day 22 at a 12-h interval. Because of the SST and radiative forcing symmetry with respect to the equator, a cloud cluster arises over the equator or a pair of cloud clusters arise near the equator. The interpretation of the poleward movement of the cloud cluster, against the equatorward low-level Hadley circulation, will be discussed in the next section. In about 5 days the cloud cluster can reach  $25^{\circ}\text{N}$  or  $\text{S}$  and eventually evolves into a midlatitude cyclone. Occasionally, before reaching midlatitude, a cloud cluster may reach the intensity of a tropical cyclone. Figure 9 shows an example of the surface pressure field on day 24, hour 6. Often at this stage upstream in the neighborhood of the equator, there is another new cloud cluster intensifying. These vortices naturally in-

duce low-level westerly wind over the equator across a broad longitudinal range very closely resembling the westerly wind burst situation. Figure 10 shows the 850-mb wind distribution at the same time as in Fig. 9 with two vortices on either side of the equator and westerly winds over the equator covering more than  $60^{\circ}$  in longitude. The observed longitudinal range of an intense westerly wind burst reaches as much as  $65^{\circ}$  (Keen 1987). Figure 11 shows the zonal wind at  $25^{\circ}\text{E}$  over the equator. It exhibits a westerly wind burst event of 20-days duration with maximum wind over  $20 \text{ m s}^{-1}$  and the westerly extends above 200 mb. High in the upper troposphere there are strong easterlies. All these numbers fall within the normally observed ranges [as presented by Lau et al. (1996) and Phoebus and Fiorino (1994)].

Figures 12 through 14 show the results of a composite of the super cloud cluster for the last 20 days in Fig. 7. The method of compositing is first to shift the results in longitudinal direction. The amount of shifting is a function of time such that the super cloud cluster becomes stationary after the shift. A time average is then taken to obtain the composite picture. This is essentially a time average in a framework moving at the speed of the super cloud cluster. The figures are centered at approximately the location where the maximum composite rainfall is at the equator. The precipitation (Fig. 12a) is about  $40^{\circ}$  wide at the equator. The spread toward northwest and southwest, which enhances the Rossby wave-like circulation component to the west of the convective region as a result of movement of twin vortex pairs, corresponds well with observation. Hendon and Salby's (1994) Fig. 4 shows such size and spread in the observed convection associated with the MJO. Sea level pressure (Fig. 12b) shows a low almost  $30^{\circ}$  east of convection center. Again, this is in agreement with observations. Madden and Julian's (1972) Fig. 16, panel a, shows exactly the same distribution of sea level pressure for the mature phase of the MJO. The amplitude of the pressure perturbation along the equator, however, is more than 3 mb, much larger than the observed 1 mb. This is likely to be related to the fact that there is only one super cloud cluster in the composite period, which accounts for all the necessary rainfall amount to balance the radiative cooling. The situation should improve when land is introduced. Stationary convective regions over the Maritime Continent, Africa, and South America can account for a good deal of rainfall such that less rainfall has to be accounted for by the super cloud cluster. Figure 10 shows the composite vertical structure of the modeled super cloud cluster. Similar to the surface pressure perturbation, the zonal wind perturbation has an amplitude of about  $10 \text{ m s}^{-1}$ , much larger than the observed  $4 \text{ m s}^{-1}$  (Madden and Julian 1972, Fig. 13). This again is likely due to the strong amplitude of the super cloud cluster and can be corrected when a full-blown GCM with continents is used. Figure 13 shows a low-level moisture maximum to the east of the maximum precipitation. This indicates that to the east of the

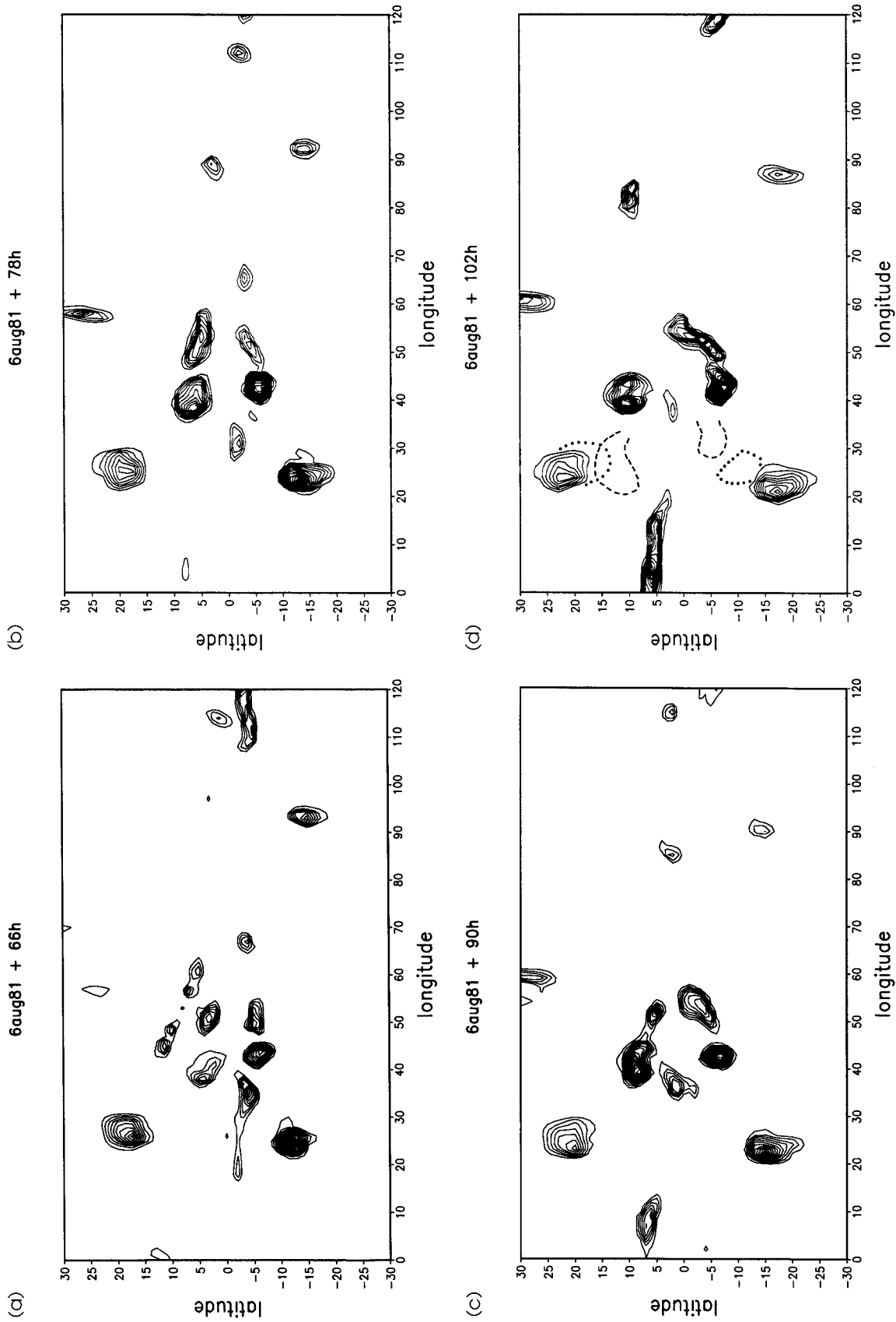


FIG. 8. Time series of precipitation (contour interval at 25 mm day<sup>-1</sup>) distribution (12-h interval) starting at day 22, hour 18, showing the poleward and weak zonal movement of cloud clusters in EMCA. The last panel shows the locations of the 25-mm day<sup>-1</sup> contour line of one vortex pair 2 days before (dotted line) and 4 days before (dashed line).

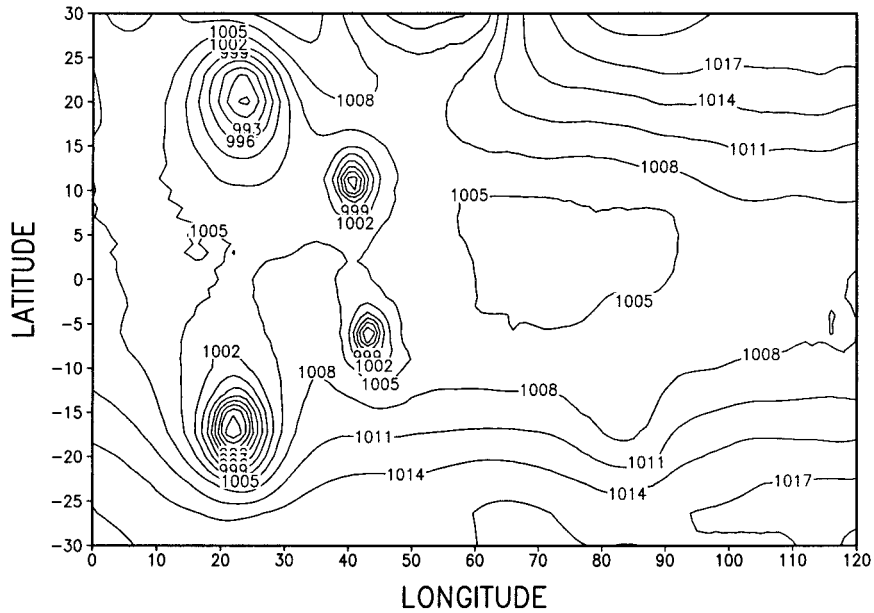


FIG. 9. The surface pressure (in mb) on day 24, hour 6 in EMCA.

super cloud cluster convective region the boundary layer air picks up moisture as it moves toward the convective region, and once inside the convective region it loses moisture due to convection. Figure 13 also shows a vertical tilt in both the convective heating field and in the vertical velocity such that the low-level convergence is ahead of the location of maximum precipitation. This is also evident in Fig. 14, which shows that the maxi-

imum 850-mb divergence is about 5° ahead of the maximum precipitation. The observed difference is about 10° (Hendon and Salby 1994). Chao and Deng (1997) discussed the origin of this out-of-phase relationship. The observed surface divergence is about 40° ahead of precipitation due to surface friction (Salby et al. 1994). Our model shows a 5° lead at the lowest level (~990 mb), but it also has a secondary divergence maximum

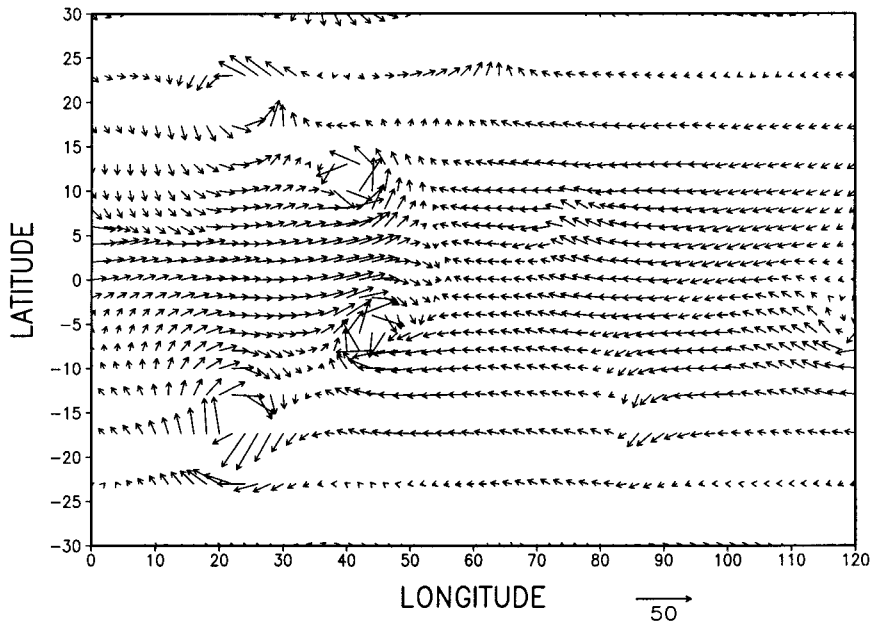


FIG. 10. The 850-mb wind ( $m s^{-1}$ ) on day 24, hour 6 in EMCA showing two pairs of vortices straddling the equator and westerly wind over the equator covering more than 60° in longitude.

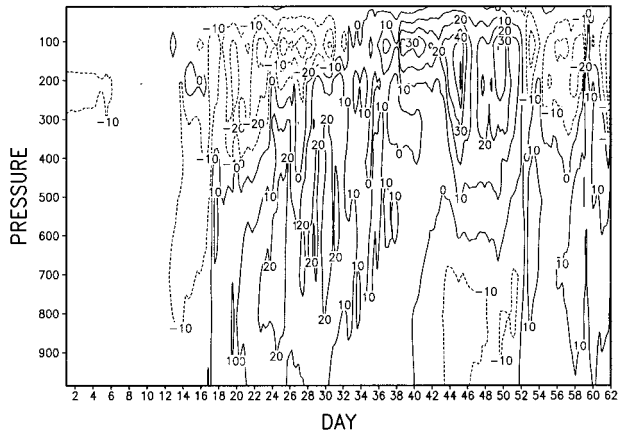


FIG. 11. Time-height distribution of zonal wind ( $\text{m s}^{-1}$ ) over the equator at  $25^\circ$  in EMCA showing a westerly wind burst event.

$32^\circ$  ahead of the precipitation maximum, and the model lowest-level divergence spreads clearly far to the east of the precipitation maximum.

This experiment, though rendering reasonable results of the super cloud clusters, cannot be considered as a completely realistic simulation of the MJO. The convective region associated with the MJO, consisting of one or more super cloud clusters, travels in only one-third of the globe (from the Indian Ocean to the mid-

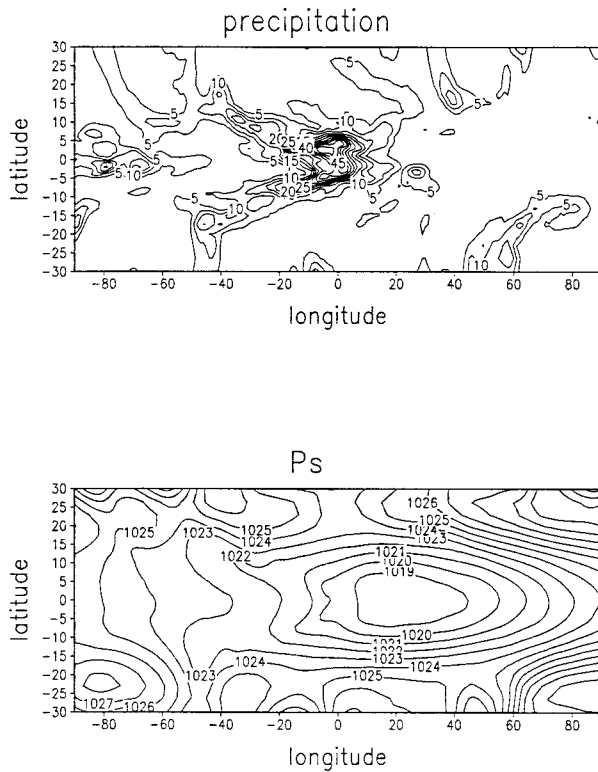


FIG. 12. Composite structure of the super cloud cluster of (a) precipitation in  $\text{mm day}^{-1}$  and (b) surface pressure in mb in EMCA.

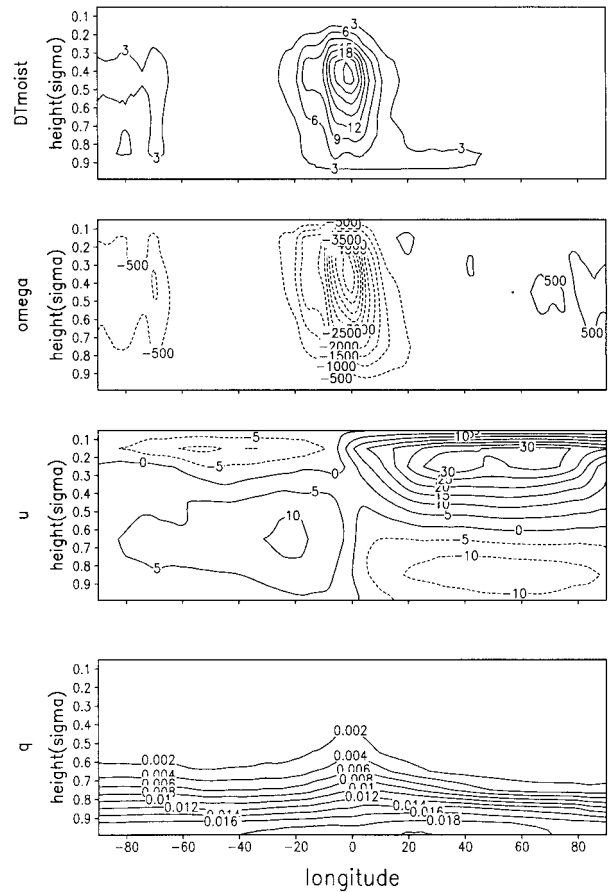


FIG. 13. Composite vertical structure along the equator of the super cloud cluster showing (a) zonal wind (in  $\text{m s}^{-1}$ ), (b) heating field (in  $^\circ\text{C day}^{-1}$ ), (c) vertical velocity in  $10^{-6} \text{ mb h}^{-1}$  in EMCA, and (d) mixing ratio in  $\text{kg kg}^{-1}$ .

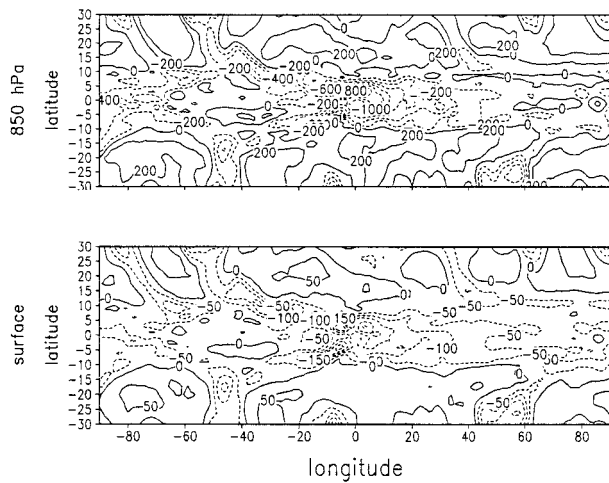


FIG. 14. Composite horizontal structure showing divergence at (a) 850 mb and (b) surface in EMCA.

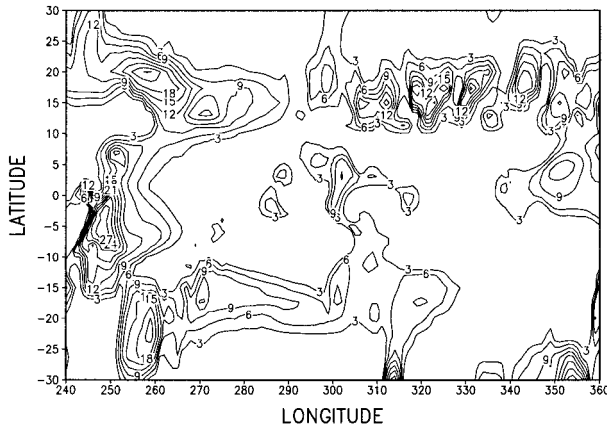


FIG. 15. Precipitation ( $\text{mm day}^{-1}$ ) distribution on day 40, hour 0 in ERAS.

Pacific) and thus cannot possibly be simulated with a zonally uniform SST distribution as used in our model. We expect that when land is introduced, there will be a good deal of improvement.

The experiment with RAS, denoted by ERAS, is identical to EMCA except that the MCA scheme is replaced by RAS. Figure 15 shows a typical precipitation field in the Tropics. It shows a very widely spread precipitation area with lower precipitation intensity. Since the precipitation has low intensity, the wind field shows very weak divergence and vorticity fields. The longitude–time plot of precipitation over the equator (Fig. 16) shows no super cloud cluster structure (in the sense that there is no sign of westward moving well-separated individual cloud clusters and eastward moving envelope of cloud clusters). The pattern difference between Figs. 16 and 7 cannot be explained away by the choice of contour lines. If the  $5 \text{ mm day}^{-1}$  contour line is not drawn in Fig. 16, the pattern before day 36 may have separate cloud clusters. However, the individual cloud cluster is clearly moving in exactly the same direction as the envelope. Also, the precipitation pattern moves eastward at a very high speed of  $30 \text{ m s}^{-1}$ , a speed that is close to the optimal speed for creating boundary convergence of a moving precipitation region (Chao 1995). These have hardly any resemblance to the observed super cloud clusters. Moreover, the vortex pairs scenarios do not exist in this experiment and, thus, westerly wind burst events do not occur. The composite precipitation pattern (Fig. 17a) shows a wider north–south extent than east–west extent contrary to the observations. Also, no protrusions in the northwest and southwest directions in the precipitation pattern are found. Overall the precipitation is much more widespread and, therefore, the intensity is much less. Correspondingly, the composite surface pressure field (Fig. 17b) shows much weaker amplitude than the EMCA case. The composite vertical structure of convective heating and vertical velocity along the equator (Fig. 18) shows no discernable phase

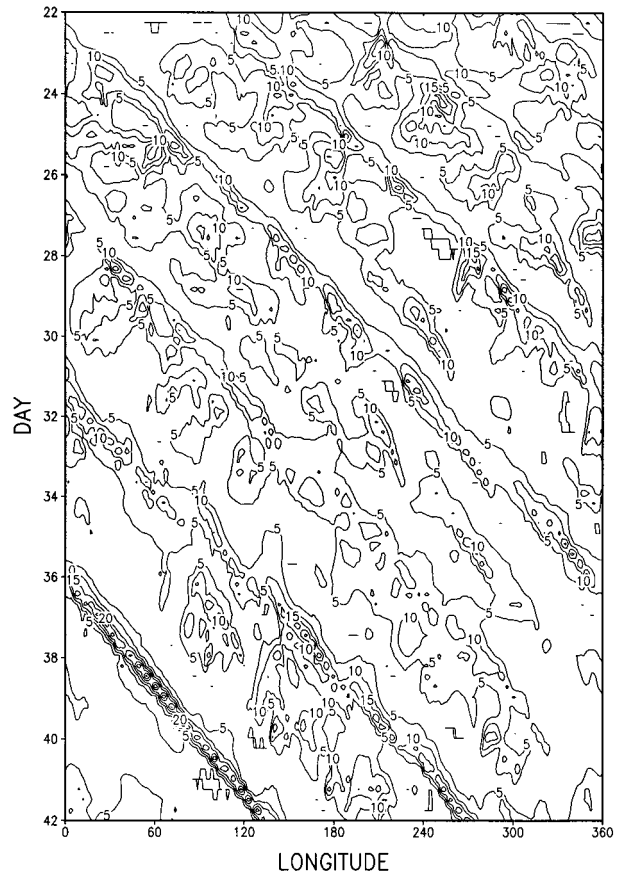


FIG. 16. Longitude–time plot of precipitation ( $\text{mm day}^{-1}$ ) averaged between  $5^{\circ}\text{S}$  and  $5^{\circ}\text{N}$  in ERAS.

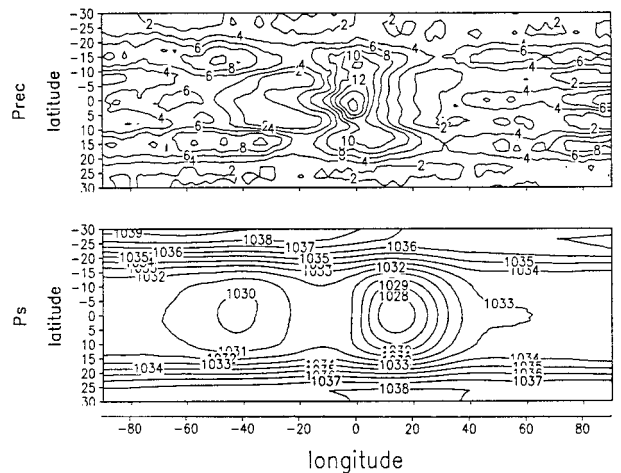


FIG. 17. Horizontal composite structure of super cloud cluster in ERAS showing (a) precipitation (in  $\text{mm day}^{-1}$ ) and (b) surface pressure (in mb).

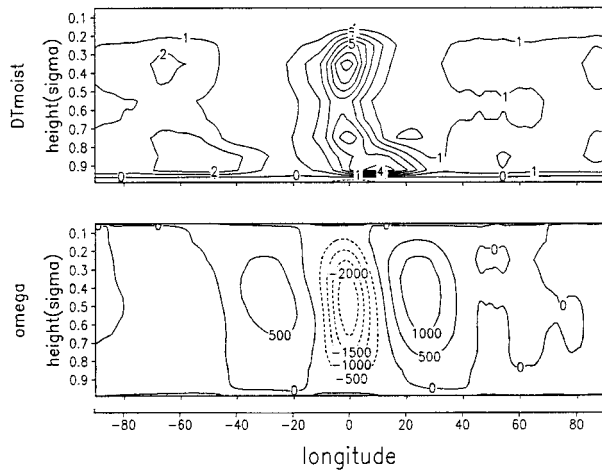


FIG. 18. Vertical composite structure along the equator of super cloud cluster in ERAS showing (a) convective heating field (in  $^{\circ}\text{C day}^{-1}$ ) and (b) vertical velocity in  $10^{-6} \text{ mb h}^{-1}$ .

lag between deep convection and low-level convergence, contrary to the observations.

The experiment with the simple convection scheme of CL, denoted by ECL, gives in the longitude–time plot of precipitation over the equator (Fig. 19) a structure that, upon close examination, does not fit the observed structure of super cloud clusters. This structure shows a pulsating cloud cluster moving eastward and shedding new westward moving cloud clusters. If the lowest contour line in Fig. 19 is not drawn, then we see some eastward moving cloud clusters along with some westward moving cloud clusters. This is distinctly different from the observations [cf. Fig. 11 of Nakazawa (1988)]. The observed super cloud cluster is the envelope of successive individual cleanly separated cloud clusters moving all in the same direction, which is distinctly different from the direction in which the envelope moves. This structure moves with a speed,  $9 \text{ m s}^{-1}$ , comparable to EMCA. The westward movement of cloud clusters with a speed of  $17 \text{ m s}^{-1}$  is realistic but obviously unlike those in EMCA. Although the cloud clusters remain at the same latitude (the equator) for longer than a day, this is shorter than the typical 2–3 days that is found in observations (Nakazawa 1988). The separation between the cloud clusters is not clean, whereas clean separation is the norm in EMCA and in nature (Figs. 5 and 11 of Nakazawa 1988). This is a second major difference from the results of EMCA. In fact, the westward moving cloud clusters are shed from a continuously eastward moving and pulsating cloud cluster (Fig. 11). “Unclean” separation between cloud clusters exists occasionally in the 2D results with the simple convection scheme (CL, Fig. 1) but not in the same manner as in the present 3D simulation. In the 2D results the neighboring cloud clusters are occasionally connected; however, the location of initiation of a new cloud cluster is distinctly separately from the existing

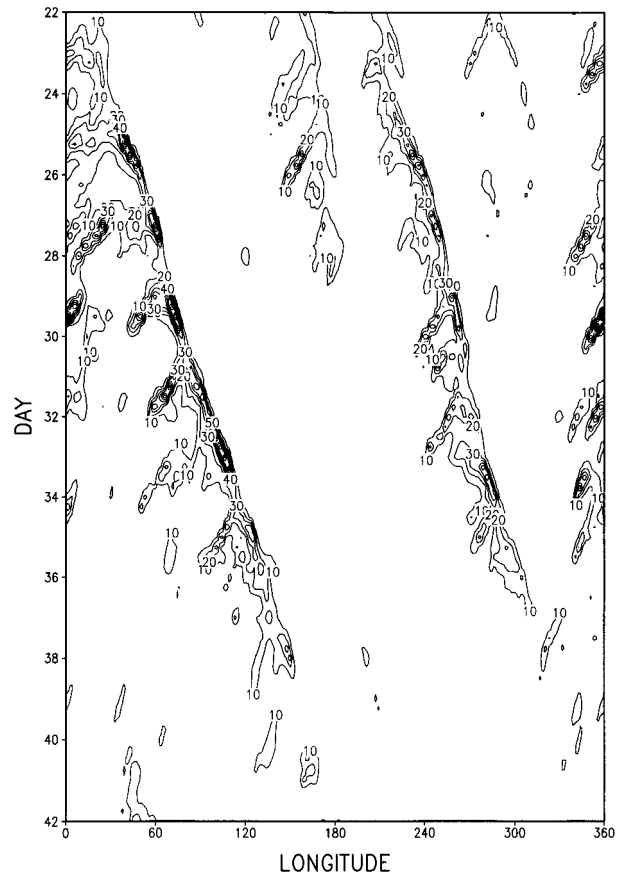


FIG. 19. Longitude–time plot of precipitation ( $\text{mm day}^{-1}$ ) averaged between  $5^{\circ}\text{S}$  and  $5^{\circ}\text{N}$  in ECL.

cloud cluster, whereas the 3D results show no such feature. Thus, we conclude that the cloud cluster tele-induction mechanism is not operating in this experiment. Thus, the super cloud cluster structure is not well simulated.

A westerly wind burst event is found in ECL. However, the eastern end of the westerly region over the equator is met by an easterly of the same kind of magnitude. The corresponding convergence coincides with the precipitation region over the equator. Figures 20a,b give a typical example of such a flow pattern and the corresponding precipitation for day 44, hour 0. They show westerly winds over the equator between longitude  $45^{\circ}$  and  $78^{\circ}$  met by easterly winds of the same magnitude on its eastern side. Such structure is quite different from reality where the easterly winds on the eastern side of a westerly (wind burst) region is much weaker (Hartten and Young 1998, manuscript submitted to *J. Climate*). This observational fact can be inferred from p. 23 of Fiorino et al. (1994). The westerly wind burst event they presented is a part of the eastward propagation of the MJO and the figure shows that prior to the occurrence of the westerly burst there is no substantial increase in the easterly wind at the equator. The observed westerly

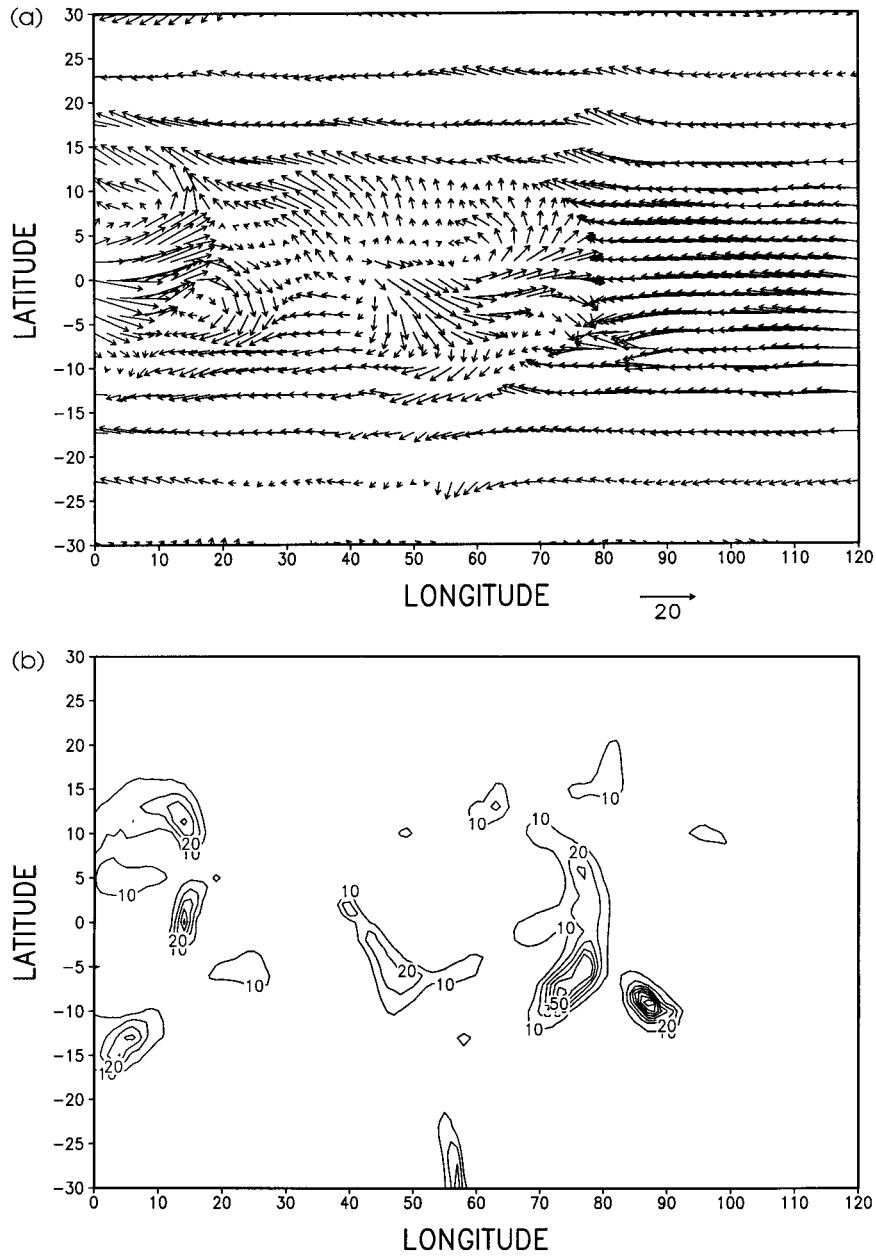


FIG. 20. (a) 850-mb wind distribution in one-third of the equatorial domain at day 44, hour 0 in ECL. (b) The corresponding precipitation pattern.

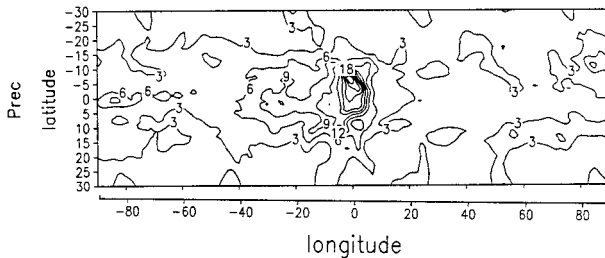


FIG. 21. Horizontal composite structure of super cloud cluster in ECL showing precipitation (in mm day<sup>-1</sup>).

wind in the westerly wind burst region is due to cyclonic vortices (and thus precipitation regions) away from the equator and not due to a large convective region over the equator. The composite precipitation (Fig. 21) in its more intense core has a wider north-south extent than east-west extent. There is little protrusion in the northwest and southwest directions. A secondary maximum over the equator lies some 25° to the west of the primary maximum, a feature not observed in the real data. The vertical structure of the convective heating (Fig. 22a) shows in the upper troposphere an extension far into the west and a secondary maximum. Correspondingly, a

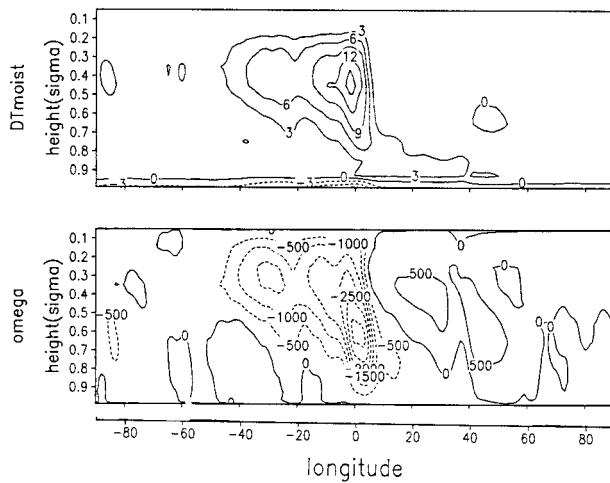


FIG. 22. Vertical composite structure of super cloud cluster in ECL showing (a) convective heating field (in  $^{\circ}\text{C day}^{-1}$ ) and (b) vertical velocity in  $10^{-6} \text{ mb h}^{-1}$ .

secondary maximum is found in the vertical velocity composite over the equator (Fig. 22b). Apparently the westward moving cloud clusters shed from the main eastward moving cloud cluster experience a growth (Fig. 19). The cause of these differences in simulating the super cloud cluster obviously has to do with the simple convection scheme used in this experiment, since the only difference between ERAS and EMCA is in the convective scheme used. The reason why the simple convection scheme is less successful in a 3D setup than in a 2D setup must have to do with the change from 2D to 3D and will be discussed in the next section.

Since EMCA is the only successful simulation thus far (albeit the absence of westward movement of cloud clusters), the next experiment is done with the MCA scheme. The effect of evaporation–surface wind feedback is revealed in an experiment where the dependence of evaporation on surface wind is removed by replacing the surface wind factor in the evaporation formula by a constant of  $5 \text{ m s}^{-1}$ . The wind factor in computing the other surface fluxes is not changed. The longitude–time distribution of precipitation in the  $5^{\circ}\text{S}$ – $5^{\circ}\text{N}$  range is shown in Fig. 23. Super cloud clusters still exist. Comparing with Fig. 7 of EMCA, one notices that the most obvious difference is that in this experiment there are more super cloud clusters quite evenly distributed. Thus, our finding is that the evaporation–surface wind feedback mechanism is not necessary for the existence of the super cloud clusters. The vortices (and thus the cloud clusters) have lower intensity in this experiment. Correspondingly, the westerly wind burst intensity is lower. Individual cloud clusters are relatively short lived. The speed of the super cloud cluster is much slower. The lower intensity of the cloud clusters is consistent with the finding that there are more cloud clusters for the reason that more weaker cloud clusters is necessary to yield the same amount of convective heating

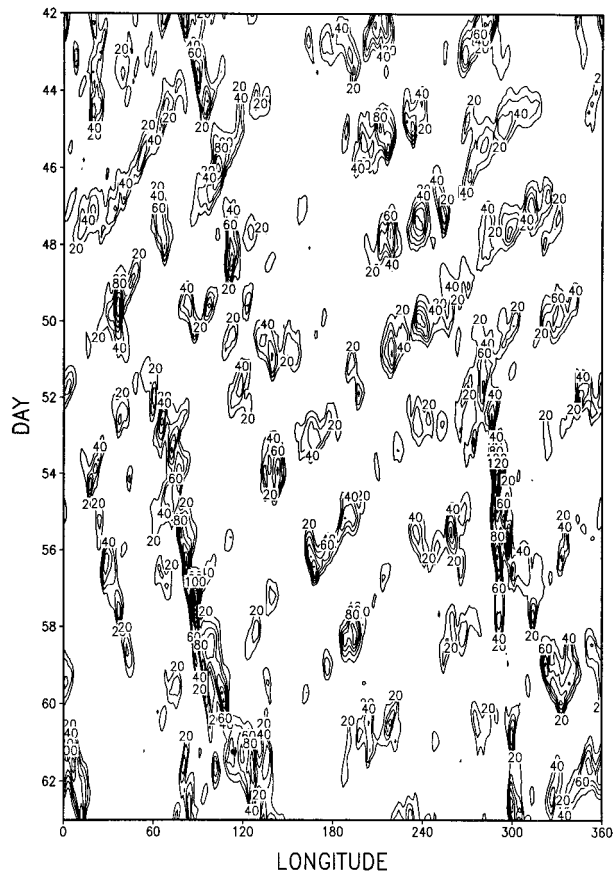


FIG. 23. Longitude–time plot of precipitation ( $\text{mm day}^{-1}$ ) averaged between  $5^{\circ}\text{S}$  and  $5^{\circ}\text{N}$  in an experiment repeating EMCA but with the evaporation–surface wind dependence removed.

to balance the imposed radiative cooling. Our results concerning the effects of evaporation–surface wind feedback are consistent with those of Neelin et al. (1987), which indicated that the MJO signal in a GCM still existed but was weaker when the evaporation–surface wind feedback is suppressed.

In our interpretation of the cloud cluster teleinduction mechanism the basic easterly flow is crucial for the mechanism to exist. An experiment was conducted to investigate the role of the basic easterly. In this experiment everything is the same as EMCA except that the zonally averaged zonal mean is set to be zero at all levels and all latitudes after every dynamics time step. The resulting precipitation pattern (Fig. 24) shows no sign of super cloud cluster structure. This is consistent with our interpretation of the teleinduction mechanism. In another experiment to investigate the role of  $\beta$ , the EMCA experiment is repeated with the Coriolis force removed and the basic zonally averaged zonal flow restored to the time-averaged zonally averaged zonal flow of EMCA after every dynamics time step. The resulting precipitation pattern (Fig. 25) shows super cloud clusters can still exist. The composite picture of this experiment shows a double ITCZ structure and no north-

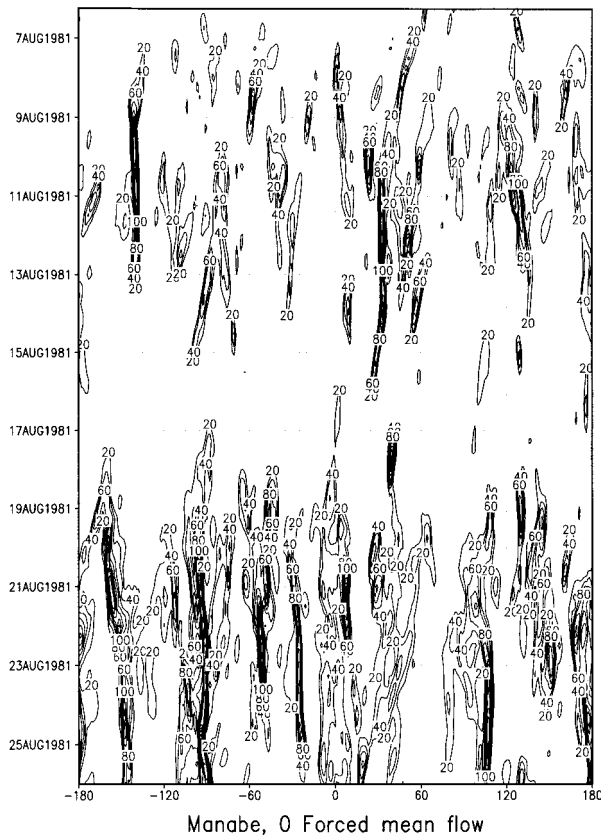


FIG. 24. The longitude–time distribution of cumulus precipitation ( $5^{\circ}\text{S}$ – $5^{\circ}\text{N}$ ) in an experiment similar to EMCA but with zonally averaged zonal wind set to zero after every time step.

westward and southwestward protrusions. Thus,  $\beta$  is not an essential element for the existence of the super cloud clusters but it is important for the horizontal shape of the composite convective region. Also from this experiment it can be concluded that the Kelvin and Rossby waves are not essential for the existence of the super cloud clusters. However, they do play important modifying roles.

#### 4. Discussion

One basic finding of our experiments is that the cloud cluster teleinduction mechanism found in a 2D model (CL), thus the super cloud cluster structure, can exist in a 3D model. An important difference between 2D and 3D results is that in the 3D results the cloud clusters do not terminate after just 2 or 3 days. They can often move poleward and westward and not infrequently move into middle latitudes. Dissipation and termination of cloud clusters in the model Tropics is also common.

Although our experiment, EMCA, shows considerable qualitative successes such as the existence of super cloud cluster, its eastward movement, the vortex pair (strong enough to be called twin cyclones), and the westerly wind burst; quantitatively our results have many

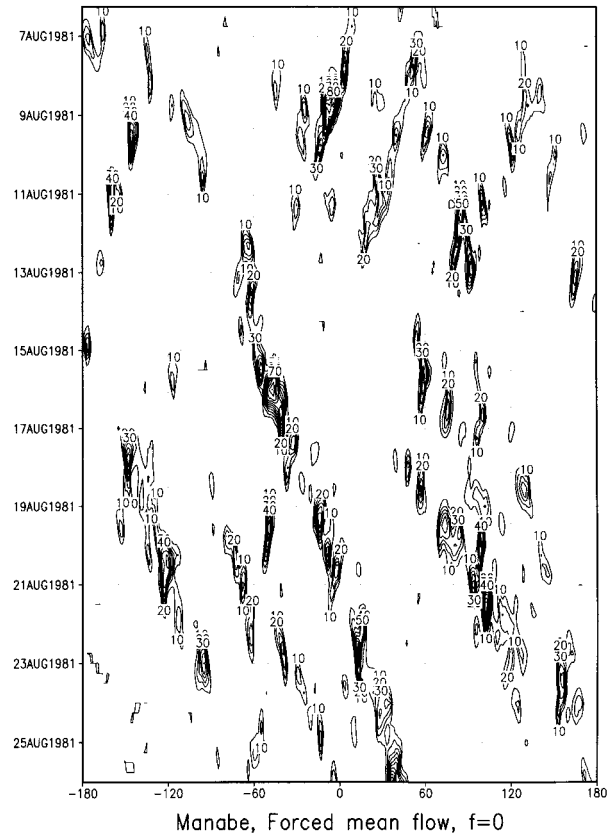


FIG. 25. The longitude–time distribution of cumulus precipitation ( $5^{\circ}\text{S}$ – $5^{\circ}\text{N}$ ) in experiment similar to EMCA but with the Coriolis force removed and the zonally averaged zonal flow restored to the time-averaged zonally averaged zonal flow of EMCA.

deficiencies. The zonal movement of the cloud cluster appears to be too small. As a result, in the longitude–time distribution of precipitation over the equator the individual cloud clusters do not exhibit westward movement as in Nakazawa's observation. It is known (Hopfinger and van Heijst 1993) that a single positive vortex of high intensity on a  $\beta$  plane moves northwestward [see also Li and Wang (1994) and references therein]. Its westward component can be diminished when it is interacting with another vortex of the same high intensity on the other side of the equator. Even without the help of another vortex on the other side of the equator, the westward movement of a vortex can be small due to  $\beta$  drift. The intensity of the vortices in our model appears to be too high. This is also evidenced by the strong pressure gradient in the vortices found in the model. The possible causes of the high vortex intensity can be numerous. Judging from the high dependence of the results on the cumulus convection scheme used in the model (soon to be presented), we can conclude that treatment of cumulus parameterization is high on the list of model components whose modification can greatly improve the model results in the sense of increasing westward movement of the cloud clusters. This is of

course hardly surprising given that what we are investigating is the interaction between convection and wind circulation. The treatment of moisture advection, which has a profound impact on the moisture distribution—part of the input parameters of the convection schemes, should also be high on the list, particularly the vertical moisture advection (Rasch and Williamson 1991). One caveat is that the sensitivity of model results to the choice of moisture transport scheme undoubtedly exists but it may have been distorted (most likely exaggerated) by the poorly formulated cumulus parameterization. Other possible causes may lie in the differences between our simplified model and the complete model.

Of the three convection schemes that we have used, only the moist convective adjustment scheme can be considered qualitatively successful in simulating the cloud cluster teleinduction mechanism responsible for the origin of the super cloud cluster structure. The reason for the more stringent requirement on the convection scheme in 3D than in 2D models has been mentioned in the introduction. Here we will discuss it further. In order for a new cloud cluster (or a cloud cluster pair) to be initiated at a location on the upstream side of an existing cloud cluster (or a cloud cluster pair) there must be strong enough uplifting at the top of the boundary layer to trigger the instability that is responsible for growth of the new cloud cluster. Such uplifting can materialize only through gravity (or, more precisely, inertio-gravity) waves excited by the existing cloud cluster (or the cloud cluster pair) at a distance. For the same degree of explosiveness in the growth of a cloud cluster the intensity of the gravity wave that is generated at a fixed distance is weaker in the 3D than in the 2D model setup, simply because of the geometry. The degree of explosiveness in the growth of a cloud cluster in a model is, of course, critically dependent upon the way cumulus convection is parameterized. The cumulus convection scheme that gives more explosive growth of the cloud clusters has a better chance of succeeding in simulating super cloud clusters. The simple convective scheme creates a lower degree of explosiveness in the growth of cloud clusters than the MCA scheme as evidenced by the lower precipitation rate associated with the cloud clusters in both the 2D simulation (Figs. 1 and 7 of CL have maximum values of 170 and 265 mm day<sup>-1</sup>, respectively, which were inadvertently not indicated in the figures) and the present 3D simulation. Thus, it fits our argument that in the 3D setup the moist convective adjustment scheme is qualitatively successful in simulating super cloud clusters, while the simple convective scheme fails. How and if the simple convective scheme can be modified in order to be successful are interesting questions, but they are not pursued in this paper.

The sensitivity of the model results to the choice of the convection scheme should not be surprising. The super cloud cluster has its origin in the cloud cluster teleinduction mechanism. The latter depends on the explosive growth of the cloud cluster to excite a gravity

wave of sufficient amplitude. How explosive the growth is depends, of course, heavily on the convection scheme. Slow growth is often associated with low peak intensity, which implies low peak precipitation intensity. RAS has the lowest maximum precipitation intensity in both 2D and 3D setups and is thus not successful in simulating super cloud clusters in both setups and this, not surprisingly, fits our argument well. Exactly why RAS gives slow cloud cluster growth rate is a fundamental question. Thus far we can only provide the following speculative discussion.

The Arakawa–Schubert (AS) scheme has the important attribute of pointing out and using the cloud work function quasi-equilibrium assumption (CWFQEA). This assumption states that the time rate of change of the cloud work function (CWF) of each cloud type is much smaller than its two component rates due to the cumulus ensemble and the large-scale processes. This assumption has the support of observational analysis (Arakawa and Schubert 1974, their Fig. 13) and cumulus ensemble model output analysis (Xu and Arakawa 1992, their Figs. 11 and 12) and is not challenged here. How to use this assumption and if it can be used in a cumulus convection scheme are questions that, in our opinion, are still unsettled. The way the AS scheme utilizes this assumption for cumulus parameterization closure purpose (Lord et al. 1982) is to set a critical CWF value (obtained from observed time-averaged CWF) for each cloud type, to let the large-scale processes in the model operate for a certain length of time (30 min or so) and to adjust the CWF of each cloud type, if it is higher than the critical value, back down to its critical value. This way of implementation keeps the model CWF of a cloud type at a fixed value in regions where a cloud type exists. Thus, this way of utilizing the CWFQEA actually does more than what this assumption dictates. The small rate of change of CWF has been turned into keeping CWF at a constant when there is convection. CWF being a constant in the presence of convection is not supported by observations. Lord and Arakawa's (1980) Fig. 9 shows that the CWF that is computed with vertical thermodynamical profiles averaged over a region even as large as the GARP Atlantic Tropical Experiment varies in time with a standard deviation as large as one-third of its time mean for tall cloud types and even greater for shallow cloud types. The same figure shows that at individual stations the standard deviation is much greater. Such temporal variation of CWF (averaged over an area the size of a model grid box) is of course largely due to the growth and decay of cloud clusters. Thus, the AS scheme's method of utilizing CWFQEA does not allow fast growth of cloud clusters. Without the rapid growth of a cloud cluster to excite strong enough gravity waves, the cloud cluster teleinduction mechanism cannot be simulated. Consequently models using the AS scheme fail to show super cloud cluster structure and the Madden–Julian oscillation. RAS does not bring the CWF to its critical value com-

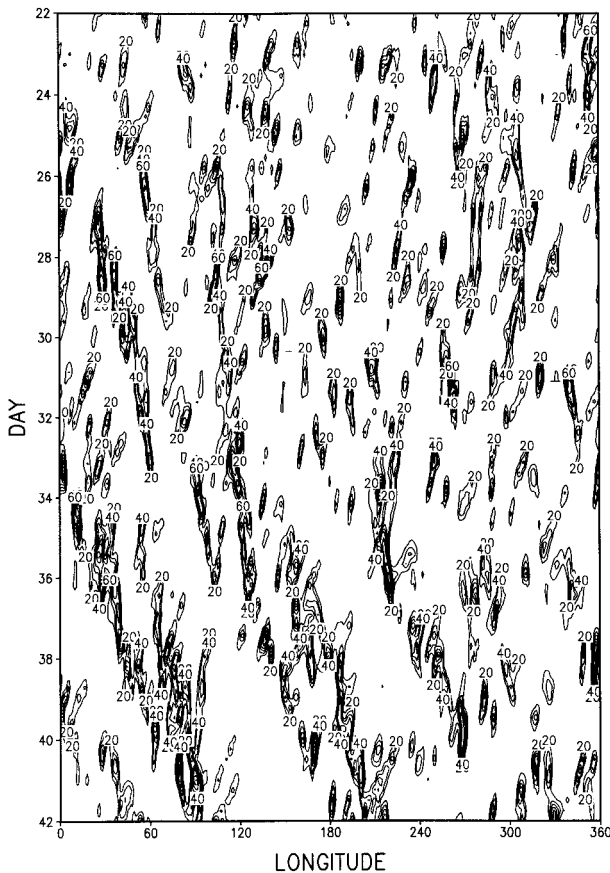


FIG. 26. Longitude–time plot of precipitation ( $\text{mm day}^{-1}$ ) averaged between  $5^{\circ}\text{S}$  and  $5^{\circ}\text{N}$  in an experiment where the cumulus parameterization is bypassed and the convection is handled by the large-scale convection.

pletely but only partially in a relaxation manner. However, this has the somewhat equivalent effect of raising the critical CWF and our experiments show that it is still very restrictive. We have increased the relaxation coefficient in RAS in 2D experiments. As the relaxation coefficient is increased, the effects of RAS diminish and eventually the large-scale convection takes over and produces super cloud clusters. We did an integration of the 3D model bypassing cumulus parameterization and allowing the large-scale convection; the resulting longitude–time distribution of precipitation averaged between  $5^{\circ}\text{S}$  and  $5^{\circ}\text{N}$  is shown in Fig. 26. Unlike EM, this figure shows super cloud clusters with more complicated internal structure. Since the large-scale convection cannot be used to replace the cumulus scheme, this integration has only academic interest.

Incidentally, the semiprognostic tests of the AS scheme, such as those of Lord (1982), Grell et al. (1991), and Xu and Arakawa (1992), do not use the approach of bringing CWF to its critical value. Thus these tests, though meaningful for testing CWFQEA, cannot be considered as tests of the AS scheme that is actually used in the models.

Obviously some change to RAS is necessary. Kuma (personal communication) has recently revised the Arakawa–Schubert scheme replacing the quasi-equilibrium closure by a prognostic method of determining the cloud-base mass flux and has been successful in obtaining super cloud cluster structure. His results still achieve a quasi equilibrium (as would any reasonable cumulus parameterization scheme) but not the same quasi equilibrium as dictated by the Lord et al. (1982) and RAS implementations of AS (we anticipate that his model results give a much larger fluctuation of the cloud work function). This concludes our speculative discussion on the failure of RAS and naturally this speculation should be further investigated.

Our simulation results clearly show that the westerly wind burst event is really an integral part of the super cloud cluster structure. Our experimental setup has symmetry with respect to the equator; thus the results often show vortex pairs across the equator. Even without such symmetry, vortices formed on one side of the equator are sufficient to give rise to westerly wind burst events over the equatorial area. Observation during the TOGA Coupled Ocean–Atmospheric Response Experiment shows a case (mid-December 1992 through early January 1993) like this (Fiorino et al. 1994, pp. 25, 43).

The surface wind–evaporation feedback mechanism is found to be unnecessary for the existence of the cloud clusters. However, it is an important factor determining the intensity of the cloud clusters. Since our simulations succeeded only in simulating super cloud clusters and cannot be considered as successful in simulating the MJO, the precise role of the surface wind–evaporation feedback mechanism in the MJO is not determined by our experiments.

Our present work of aquaplanet simulations represents an outgrowth of previous work on this subject. The work by Hayashi and Sumi (1986) obtained eastward movement of convective regions but not the westward movement of the individual cloud clusters. Numaguti and Hayashi (1991a) did a similar numerical simulation with MCA. Judging from their Fig. 13, we note that they did obtain super cloud clusters with comparable speed ( $8.5 \text{ m s}^{-1}$  vs our  $10 \text{ m s}^{-1}$ ). Their results show strong planetary wavenumbers 1 and 2, similar to our results. The zonally averaged precipitation over the equator is less than  $4 \text{ mm day}^{-1}$  (their Fig. 12 vs our  $10.2 \text{ mm day}^{-1}$ ). The closeness of their results to ours is quite encouraging. The quantitative differences between their results and ours only point out the sensitivity of the simulation to different model designs and parameters. Both papers attributed the origin of the eastward movement to Kelvin wave–CISK, which was critically reviewed by Chao (1995).

At the conclusion of our experiments we became aware of Kuma's (1994) simulations with the Japan Meteorological Agency global spectral model on an aquaplanet. Kuma used full physics including a revised Kuo scheme. To a high degree his results are consistent with

ours. He, too, obtained one or two super cloud clusters most of the time, which travel around the globe in about 40 days (a speed three times that of the observed convective region associated with the MJO). His results of super cloud clusters giving rise to cyclogenesis is the same as what we obtained. One striking difference is that the zonal component of movement of the individual cloud clusters in his simulation is more realistic than ours, which is too slow. The cause for this difference is likely to be in the cumulus convection schemes used, though the precise cause requires further study. His results clearly show the importance of high horizontal resolution and the model's capability of simulating the life cycle of individual cloud clusters as emphasized in CL.

Recently in a complementary study Yano et al. (1995) have simulated hierarchical tropical cloud systems in a shallow-water system. They also obtained the high sensitivity of the simulations to the choice of convection scheme. The speed of their super cloud clusters, 22 days to circle the globe, is higher than what we obtained in EMCA. This may be improved by changing their model parameters. They have stated that the WISHE mechanism that they rely on for explanation did not work for some cases. Contrary to observations, their individual cloud clusters have a pulsation period shorter than 1 day. This is likely to be related to the convection schemes used. The circulation pattern they obtained has a bow-shaped cloud cluster racing eastward and shedding new cloud clusters behind, a result quite similar to our ECL (Figs. 19 and 20b) and is different from the observed pattern and from what we have obtained in EMCA. Thus, their results can be improved by improvement in their treatment of convection parameterization.

## 5. Summary and remarks

In extending CL's work, we have simulated the super cloud cluster and westerly wind burst events in a 3D aquaplanet setting. As an integral part of super cloud clusters, the westerly wind burst is due to two or more successive cloud clusters pairs (vortex pairs, or twin cyclones) straddling the equator that are generated by a cloud cluster teleinduction mechanism. When SST is not symmetric with respect to the equator, vortices may occur in one hemisphere only; but that is sufficient to give rise to westerly wind bursts. Of the three cumulus convection schemes tried, the MCA scheme performed best for our purpose. To the extent that cloud cluster teleinduction, cloud cluster pairs in the north-south direction, and the subsequent development of a westerly wind burst appeared in our simulation, we achieved a modest qualitative success. The speed of the super cloud clusters in our model is reasonable compared with what is observed. However, our model results do not show a group of super cloud clusters packed together to form a convective region associated with the MJO (the ob-

served packing is demonstrated by Nakazawa 1988). Thus, our simulations cannot be considered as a completely successful simulation of the MJO. Also, the observational study by Hendon and Liebmann (1994) has questioned the importance of the super cloud cluster in the origin of the MJO, in contrast with our emphasis on the role of the super cloud clusters. The resolution of these problems will be one of our important future goals.

The evaporation-surface wind feedback is found to be unnecessary for the existence of the super cloud clusters and their internal structure, although it does affect their intensity. Our results demonstrate the crucial role of the cumulus convection scheme, and the greater demand on the cumulus convection scheme in the 3D setup than in the 2D setup. Moreover,  $\beta$  is found not to be important to the genesis of the super cloud clusters and has only modifying effects. However, it should be mentioned that the basic easterly wind owes its existence to the earth's rotation, which is related to  $\beta$ .

The qualitative success of the MCA scheme for our present purposes should not be used as support for the use of the MCA scheme for general circulation modeling in general. Certainly the MCA scheme has its own drawbacks when viewed from other perspectives. For example, the MCA scheme has no capability of moving boundary layer mass directly into the upper troposphere in the "protected core" (the so-called hot towers), whereas the AS scheme does. Other criticisms of MCA can be found in Frank and Molinari (1993). So the larger lesson that should be learned from our study is that more effort should be put into cumulus parameterization. An important part of this effort should be an intensive theoretical study of the interaction of cumulus ensembles with the large-scale circulation.

This investigation will be further extended in several directions. The observed splitting of a cloud cluster over the equator, after being created through the teleinduction mechanism, into a north-south pair is an interesting topic, so are the factors that determine the meridional and zonal propagation speeds of the cloud clusters. The sensitivity of the model results to different SST distribution may be a fruitful investigation. These will all contribute to achieving our ultimate goal of a comprehensive interpretation of the MJO.

*Acknowledgments.* We thank our past and present colleagues in the GLA GCM modeling group for developing the GCM. Thanks are also extended to K.-M. Lau for discussion. Financial support, managed by Kenneth Bergman and Ramesh Kakar, from NASA Mission to Planet Earth Division as a part of NASA's participation in the TOGA COARE program was indispensable.

## REFERENCES

- Arakawa, A., and W. H. Schubert, 1974: The interaction of a cumulus cloud ensemble with the large-scale environment. Part I. *J. Atmos. Sci.*, **31**, 674-701.

- , and M. J. Suarez, 1983: Vertical differencing of the primitive equations in sigma coordinates. *Mon. Wea. Rev.*, **111**, 34–35.
- Chang, C. P., and H. Lim, 1988: Kelvin wave–CISK. A possible mechanism for the 30–50 day oscillations. *J. Atmos. Sci.*, **45**, 1709–1720.
- Chao, W. C., 1987: On the origin of the tropical intraseasonal oscillation. *J. Atmos. Sci.*, **44**, 1940–1949; Corrigendum, **45**, 1283.
- , 1995: A critique of wave–CISK as the explanation for the 40–50 day tropical intraseasonal oscillation. *J. Meteor. Soc. Japan*, **73**, 677–684.
- , and S.-J. Lin, 1994: Tropical intraseasonal oscillation, super cloud clusters, and cumulus convection schemes. *J. Atmos. Sci.*, **51**, 1282–1297.
- , and L. Deng, 1997: Phase lag between deep cumulus convection and low-level convergence in tropical synoptic-scale systems. *Mon. Wea. Rev.*, **125**, 549–559.
- Emanuel, K. A., 1987: An air–sea interaction model of intraseasonal oscillation in the tropics. *J. Atmos. Sci.*, **44**, 2324–2340.
- , J. D. Neelin, and C. S. Bretherton, 1994: On large-scale circulations in convecting atmospheres. *Quart. J. Roy. Meteor. Soc.*, **120**, 111–1143.
- Ferranti, L., T. N. Palmer, F. Molteni, and E. Klinker, 1990: Tropical–extratropical interaction associated with the 30–60 day oscillation and its impact on medium and extended range prediction. *J. Atmos. Sci.*, **47**, 2177–2199.
- Fiorino, M., S. J. Lord, W. K.-M. Lau, P. A. Phoebus, and C. G. Strey, 1994: A synoptic-scale overview of the TOGA COARE intensive observing period November 1992–February 1993 based on analyses from U. S. operational global data assimilation systems. NASA Tech. Memo. 104593, 288 pp. [Available from Goddard Space Flight Center, Greenbelt, MD 20771.]
- Frank, W. M., and J. Molinari, 1993: Convective adjustment. chapter 8, *The Representation of Cumulus Convection in Numerical Models*, K. A. Emanuel and D. J. Raymond, Eds. *Meteor. Monogr.*, No. 46, Amer. Meteor. Soc., 101–106.
- Grell, G., Y.-H. Kuo, and R. J. Pasch, 1991: Semiprognostic tests of cumulus parameterization schemes in the middle latitudes. *Mon. Wea. Rev.*, **119**, 5–31.
- Hayashi, Y.-Y., and A. Sumi, 1986: The 30–40 day oscillations simulated in an “aqua-planet” model. *J. Meteor. Soc. Japan*, **64**, 451–467.
- , and D. G. Golder, 1993: Tropical 40–50 and 25–30 day oscillations appearing in realistic and idealized GFDL climate model and the ECMWF dataset. *J. Atmos. Sci.*, **50**, 464–494.
- Hendon, H. H., 1988: A simple model of the 40–50 day oscillation. *J. Atmos. Sci.*, **45**, 569–584.
- , and B. Liebmann, 1994: Organization of convection within the Madden–Julian oscillation. *J. Geophys. Res.*, **99**, 8073–8083.
- , and M. L. Salby, 1994: The life cycle of the Madden–Julian oscillation. *J. Atmos. Sci.*, **51**, 2225–2237.
- Hopfinger, E. J., and G. J. F. van Heijst, 1993: Vortices in rotating fluids. *Annu. Rev. Fluid Mech.*, **25**, 241–289.
- Kalnay, E., R. Balgovich, W. Chao, D. Edlmann, J. Pfaendner, L. Takacs, and K. Takano, 1983: Documentation of the GLAS fourth-order general circulation model. Vol. 1: Model documentation. NASA Tech. Memo. 86064. [Available from Goddard Space Flight Center, Greenbelt, MD 20771.]
- Keen, R. A., 1987: Equatorial westerlies and the southern oscillation. *Proc. U.S. TOGA Western Pacific Air–Sea Interaction Workshop*, Honolulu, Hawaii, UCAR, 121–140.
- Kuma, K., 1994: The Madden and Julian oscillation and tropical disturbances in an aqua-planet version of JMA global model with T63 and T159 resolution. *J. Meteor. Soc. Japan*, **72**, 147–172.
- Lau, K.-M., and L. Peng, 1987: Origin of low-frequency oscillations in the tropical atmosphere. Part I: Basic theory. *J. Atmos. Sci.*, **44**, 950–972.
- , T. Nakazawa, and C. H. Sui, 1991: Observations of cloud cluster hierarchies over the tropical western Pacific. *J. Geophys. Res.*, **96** (Suppl.), 3197–3208.
- , P. J. Sheu, S. Schubert, and D. Ledvina, 1996: Evolution of large-scale feature during TOGA COARE based on 4D data assimilation. *J. Climate*, **9**, 986–1003.
- Lau, N.-C. and K.-M. Lau, 1986: The structure and propagation of intraseasonal oscillations appearing in a GFDL general circulation model. *J. Atmos. Sci.*, **43**, 2023–2047.
- Li, X., and B. Wang, 1994: Barotropic dynamics of the beta gyres and beta drift. *J. Atmos. Sci.*, **51**, 746–756.
- Lin, S.-J., W. C. Chao, Y. C. Sud, and G. K. Walker, 1994: A class of the van Leer–type transport schemes and its application to the moisture transport in a general circulation model. *Mon. Wea. Rev.*, **122**, 1575–1593.
- Lord, S. J., 1982: Interaction of a cumulus cloud ensemble with the large-scale environment. Part III: Semi-prognostic test of the Arakawa–Schubert cumulus parameterization. *J. Atmos. Sci.*, **39**, 88–103.
- , W. C. Chao, and A. Arakawa, 1982: Interaction of a cumulus cloud ensemble with the large-scale environment. Part IV: The discrete model. *J. Atmos. Sci.*, **39**, 104–113.
- Louis, J.-F., 1979: A parametric model of vertical eddy fluxes in the atmosphere. *Bound.-Layer Meteor.*, **17**, 187–202.
- Madden, R. A., 1986: Seasonal variations of the 40–50 day oscillation in the tropics. *J. Atmos. Sci.*, **43**, 3138–3158.
- , and P. R. Julian, 1971: Detection of a 40–50 day oscillation in the zonal wind in the tropical Pacific. *J. Atmos. Sci.*, **28**, 702–708.
- , and —, 1972: Description of global scale circulation cells in the tropics with a 40–50 day period. *J. Atmos. Sci.*, **29**, 1109–1123.
- , and —, 1994: Observations of the 40–50 day tropical oscillation—A review. *Mon. Wea. Rev.*, **122**, 814–837.
- Manabe, S., J. Smagorinsky, and R. F. Strickler, 1965: Simulated climatology of a general circulation model with a hydrological cycle. *Mon. Wea. Rev.*, **93**, 769–798.
- Moorthi, S., and M. J. Suarez, 1992: Relaxed Arakawa–Schubert: A parameterization of moist convection for general circulation models. *Mon. Wea. Rev.*, **120**, 978–1002.
- Nakazawa, T., 1988: Tropical super clusters within intraseasonal variations over the western Pacific. *J. Meteor. Soc. Japan*, **66**, 823–839.
- Neelin, J. D., and J.-Y. Yu, 1994: Modes of tropical variability under convective adjustment and the Madden–Julian oscillation. Part I: Analytical theory. *J. Atmos. Sci.*, **51**, 1876–1894.
- , I. M. Held, and K. H. Cook, 1987: Evaporation–wind feedback and low-frequency variability. *J. Atmos. Sci.*, **44**, 2341–2348.
- Newell, R. E., J. W. Kidson, D. G. Vincent, and G. J. Boer, 1972: *The General Circulation of the Tropical Atmosphere and Interactions with Extratropical Latitudes*. Vol. 2. The MIT Press, 371 pp.
- Numaguti, A., and Y.-Y. Hayashi, 1991a: Behavior of cumulus activity and the structures of circulations in an “aqua planet” model. Part I. The structure of the super clusters. *J. Meteor. Soc. Japan*, **69**, 541–561.
- , and —, 1991b: Behavior of cumulus activity and the structures of circulations in an “aqua planet” model. Part II. Eastward-moving planetary scale structure and the intertropical convergence zone. *J. Meteor. Soc. Japan*, **69**, 563–579.
- Park, C. K., D. M. Straus, and K.-M. Lau, 1990: An evaluation of the structure of tropical intraseasonal oscillations in three general circulation models. *J. Meteor. Soc. Japan*, **68**, 403–417.
- Phoebus, P. A., and M. Fiorino, 1994: Comparison of synoptic fields from the U.S. operational global data assimilation systems during the TOGA COARE IOP. TOGA Notes, No. 16. [Available from witte@ocean.nova.edu]
- Pitcher, E. J., and J. E. Geisler, 1987: The 40–50 day oscillation in a perpetual January simulation with a general circulation model. *J. Geophys. Res.*, **92**, 11 971–11 978.
- Rasch, P. J., and D. L. Williamson, 1991: The sensitivity of a general circulation model climate to the moisture transport formulation. *J. Geophys. Res.*, **96**, 13 123–13 137.
- Salby, M. L., and H. H. Hendon, 1994: Intraseasonal behavior of

- clouds, temperature, and motion in the Tropics. *J. Atmos. Sci.*, **51**, 2207–2224.
- , R. B. Garcia, and H. H. Hendon, 1994: Planetary-scale circulations in the presence of climatological and wave-induced heating. *J. Atmos. Sci.*, **51**, 2344–2367.
- Slingo, J. M., and R. A. Madden, 1991: Characteristics of the tropical intraseasonal oscillation in the NCAR community climate model. *Quart. J. Roy. Meteor. Soc.*, **117**, 1129–1169.
- Staniforth, A. N., and H. L. Mitchell, 1978: A variable-resolution finite-element technique for regional forecasting with the primitive equations. *Mon. Wea. Rev.*, **106**, 439–447.
- Sui, C.-H., and K.-M. Lau, 1992: Multi-scale phenomena in the tropical atmosphere over the western Pacific. *Mon. Wea. Rev.*, **120**, 407–430.
- Swinbank, R., T. N. Palmer, and M. K. Davey, 1988: Numerical simulations of the Madden and Julian oscillations. *J. Atmos. Sci.*, **45**, 774–788.
- Takacs, L., and R. Balgovid, 1983: High latitude filtering in global grid point models. *Mon. Wea. Rev.*, **111**, 2005–2015.
- Talagrand, O., 1972: On the damping of high-frequency motions in four-dimensional assimilation of meteorological data. *J. Atmos. Sci.*, **29**, 1571–1574.
- Tokioka, T., K. Yamazaki, A. Kitoh, and T. Ose, 1988: The equatorial 30–60 day oscillation and the Arakawa–Schubert penetrative cumulus parameterization. *J. Meteor. Soc. Japan*, **66**, 883–901.
- Wang, B., and H. Rui, 1990: Synoptic climatology of transient tropical intraseasonal convection anomalies: 1975–1985. *Meteor. Atmos. Phys.*, **44**, 43–61.
- Xu, K.-M., and A. Arakawa, 1992: Semiprognostic tests of the Arakawa–Schubert cumulus parameterization using simulated data. *J. Atmos. Sci.*, **49**, 2421–2436.
- Yano, J.-I., J. C. McWilliams, M. W. Moncrieff, and K. A. Emanuel, 1995: Hierarchical tropical cloud systems in an analog shallow-water model. *J. Atmos. Sci.*, **52**, 1723–1742.
- Yasunari, T., 1981: Structure of an Indian summer monsoon system with around 40 day period. *J. Meteor. Soc. Japan*, **59**, 336–354.
- Yu, J.-Y., and J. D. Neelin, 1994: Modes of tropical variability under convective adjustment and the Madden–Julian oscillation. Part II: Numerical results. *J. Atmos. Sci.*, **51**, 1895–1914.
- Zhu, B., and B. Wang, 1993: The 30–60-day convection seesaw between the tropical Indian and western Pacific Oceans. *J. Atmos. Sci.*, **50**, 184–199.